JP Journal of Heat and Mass Transfer

https://pphmjopenaccess.com
https://doi.org/10.17654/0973576325047 **P-ISSN: 0973-5763**
Volume 38, Number 6, December 2025, Pages 897-917 **E-ISSN: 3049-2556**

UNSTEADY MHD CASSON FLUID FLOW AND HEAT TRANSFER WITH SLIP AND THERMAL RADIATION OVER AN EXPONENTIALLY STRETCHING SHEET: A HAM-BASED STUDY

Sumitra Kakumanu and Venkata Subrahmanyam Sajja*

Department of Engineering Mathematics
Koneru Lakshmaiah Education Foundation
Guntur-522302, Andhra Pradesh, India
e-mail: subrahmanyam@kluniversity.in

Abstract

We investigate the time-dependent boundary layer flow and heat transfer behavior of a Casson fluid over an exponentially stretching surface embedded in a porous medium. The model integrates essential physical effects, including Joule heating, thermal radiation, velocity and thermal slip conditions, to enhance the physical realism of the system. The governing partial differential equations are transformed into a system of nonlinear ordinary differential equations using appropriate similarity transformations. These transformed equations

Received: August 18, 2025; Accepted: November 6, 2025
Keywords and phrases: Casson fluid, MHD, slip conditions, thermal radiation, HAM method.
*Corresponding author
Communicated by K. K. Azad

How to cite this article: Sumitra Kakumanu and Venkata Subrahmanyam Sajja, Unsteady MHD Casson fluid flow and heat transfer with slip and thermal radiation over an exponentially stretching sheet: a HAM-based study, JP Journal of Heat and Mass Transfer 38(6) (2025), 897-917. https://doi.org/10.17654/0973576325047

Published Online: December 11, 2025

are then analytically solved using the homotopy analysis method (HAM), which offers series solutions with controllable convergence. A detailed parametric analysis is carried out to explore the influence of magnetic field strength, porous medium permeability, Prandtl number, Eckert number, and thermal radiation on the velocity and temperature distributions. The findings reveal that magnetic effects and porous resistance markedly reduce the fluid velocity, whereas Joule heating and thermal radiation enhance the overall heat transfer process. Furthermore, expressions for the skin friction coefficient and Nusselt number are derived and analyzed. This study offers valuable insights applicable to advanced thermal systems, polymer extrusion, and biomedical fluid engineering involving non-Newtonian fluids.

1. Introduction

In recent years, boundary-layer flows involving non-Newtonian fluids have gained substantial attention because of their importance in numerous engineering and industrial fields, such as polymer processing, food manufacturing, paper production, and biomedical engineering. Between the many models developed to describe non-Newtonian behavior, the Casson liquid model is particularly notable for its ability to simulate shear-thinning effects and yield stress characteristics. This makes it especially suitable for modeling the flow of blood, where the formation of rouleaux structures among red blood cells introduces yield stress effects. Animasaun et al. [1] studied Casson fluid flow through stenosed arteries to emulate physiological blood flow. The Casson model behaves as an elastic solid below a particular shear stress threshold, then transitions to a fluid state as the stress increases. It exhibits infinite viscosity at zero shear rate and negligible viscosity under high shear conditions. Common examples of Casson-type fluids include blood, honey, ketchup, and fruit juices.

The flow induced by a stretching surface exponentially plays a vital role in a wide range of technological processes such as plastic film extrusion, glass fiber production, crystal growth, and the design of heat exchangers. Sakiadis [2] investigated momentum and thermal behavior in viscoelastic fluids over stretching sheets. These investigations are crucial for processes

like polymer sheet extrusion and thin film production. Traditional studies often assume a linear velocity-stretching relationship; however, Gupta and Gupta [3] noted that stretching may follow a nonlinear or exponential profile in real-world applications, especially in metal wire annealing or polymer cooling. The rate of heat transfer, influenced by exponential variations in velocity and surface temperature, is critical in ensuring product quality. Heat transport and boundary layer flow towards a porous exponential stretching sheet are described analytically by Mukhopadhyay and Gorla [4]. In place of no-slip conditions at the interface, velocity and thermal slips are taken into account.

The role of magnetic fields in boundary layer flow has also been extensively explored. Tashtoush and Al-Odat [5] investigated the influence of a magnetic field on the flow and heat transfer over an exponentially stretching sheet. Similarly, Sajid and Hayat [6] applied the HAM to investigate thermal radiation effects in such flows. Vinod et al. [7] analyzed the magnetohydrodynamic (MHD) boundary-layer flow and heat transfer characteristics of a Casson non-Newtonian fluid over an exponentially stretching sheet.

Thermal radiation significantly influences heat transfer, especially in high-temperature environments such as space missions and advanced manufacturing. Mukhopadhyay et al. [8] noted that this phenomenon plays a vital role in polymer processing, nuclear reactor operations, liquid-metal flows, and various energy-generation systems. Ishak [9] investigated radiation effects on viscous fluid flow over exponentially stretching sheets, while Bhattacharyya [10] analyzed steady boundary layer behavior under reactive mass transfer. Hayat et al. [11] explored steady MHD flow of nanofluids from porous, exponentially stretching surfaces.

Heat transfer in porous space has wide applications in engineering of geothermal, petroleum recovery, and environmental remediation. Vajravelu [12] examined flow constant and heat behavior of viscous fluids in porous environments using various thermal conditions. Abbas et al. [13] studied MHD flow on an exponentially stretched surface considering radiation and

Darcy's resistance, utilizing the HAM. Ahmad et al. [14] analyzed thermal and flow characteristics of a permeability due to stretching surface exponentially, while Srinivasacharya and Jagadeeshwar [15] incorporated convective boundary conditions and Joule heating into their model.

Several studies have also addressed unsteady flows of Casson fluids over stretching surfaces. Mukhopadhyay et al. [16] explored time-dependent flows with prescribed surface temperatures, while Ullah et al. [17] considered magnetic effects, Brownian motion, and thermophoresis in buoyancy-driven Casson fluid flows. Elbashbeshy et al. [18] provided numerical insight into suction effects under exponential temperature profiles. Additional studies by Hayat et al. [19] and Hussain et al. [20] contributed further understanding of three-dimensional and magnetically influenced flows in porous media.

Building upon previous investigations, this study further advances the analysis of Casson fluid flow by incorporating additional physical effects that are highly relevant to modern thermal-fluid applications. Specifically, it explores the unsteady, two-dimensional boundary layer behavior of a Casson liquid flowing over an exponentially stretching surface within a porous medium under the influence of a transverse magnetic field. The governing model is enhanced through the inclusion of Joule heating, nonlinear thermal radiation, and velocity and temperature slip boundary conditions, making it more representative of real-world engineering and biomedical systems. The resulting system of nonlinear partial differential equations is transformed into ordinary differential equations using similarity transformations. These transformed equations are then analytically solved using the homotopy analysis method (HAM), which provides a powerful framework to obtain convergent series solutions for complex, highly nonlinear flow problems. A comprehensive analysis is conducted to assess the effect of different parameters on velocity and heat fields, and also shear stress and heat transfer rate. The obtained results are benchmarked against existing literature to validate the accuracy and robustness of the proposed model.

2. Mathematical Model

A mathematical model is constructed to represent the unsteady flow dynamics and two-dimensional boundary layer behavior of an incompressible Casson liquid over an exponentially stretching surface embedded in a porous medium and exposed to a transverse magnetic field. The formulation incorporates key physical phenomena such as velocity slip, Joule heating, and nonlinear thermal radiation, thereby extending earlier models. By applying suitable similarity transformations, the governing partial differential equations are reduced to a coupled system of nonlinear ordinary differential equations. These equations are then solved analytically using the homotopy analysis method (HAM), which offers flexibility and control over convergence without linearization or discretization. A detailed parametric study is performed to explore the effects of various flow and thermal parameters on velocity and temperature distributions. Furthermore, expressions for skin friction and Nusselt number are derived and compared with available results to validate the accuracy and effectiveness of the proposed model.

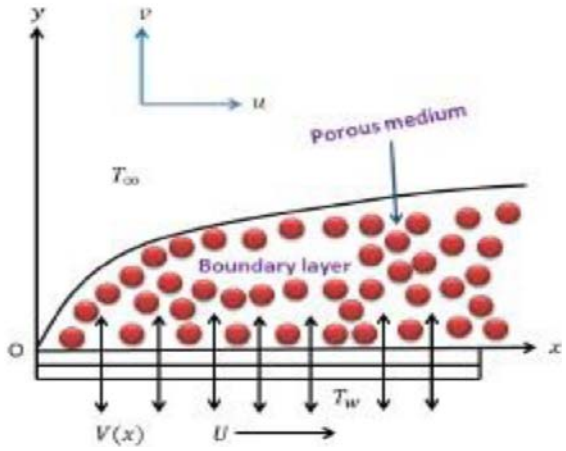

Figure 1. Flow geometry.

The equations for momentum and heat conservation are formulated based on the principles of fluid dynamics and heat transfer:

$$\frac{\partial u}{\partial x} + \frac{\partial v}{\partial y} = 0, \tag{1}$$

$$\frac{\partial u}{\partial t} + u\frac{\partial u}{\partial x} + v\frac{\partial u}{\partial y} = \nu\left(1 + \frac{1}{\beta}\right)\frac{\partial^2 u}{\partial y^2} - \frac{\sigma B_0^2}{\rho}u - \frac{\nu}{K}u, \tag{2}$$

$$\frac{\partial T}{\partial t} + u\frac{\partial T}{\partial x} + v\frac{\partial T}{\partial y} = \frac{k}{\rho C_p}\frac{\partial^2 T}{\partial y^2} + \frac{\mu}{\rho C_p}\left(\frac{\partial u}{\partial y}\right)^2 + \frac{\sigma B_0^2}{\rho c_p}u^2$$

$$+ \frac{Q}{\rho C_p}(T - T_\infty) - \frac{1}{\rho C_p}\frac{\partial q_r}{\partial y}. \tag{3}$$

By applying the approximation of Rosseland for thermal radiation, we obtain the modified heat flux expression

$$q_r = -\frac{4\sigma}{3K^*}\frac{\partial T^4}{\partial y} \approx -\frac{16\sigma T_\infty^3}{3K^*}\frac{\partial T}{\partial y},$$

Appropriate boundary conditions:

$$u = U_w(x, t),\ v = -V(x, t),\ T = T_w(x, t) \text{ as } y = 0,$$

$$u = 0,\ T = T_\infty \text{ as } y \to \infty. \tag{4}$$

Using the subscripts (∞) (ambient) and (w) (wall) to denote conditions in the free stream at the sheet, respectively, the boundary conditions presented in equation (4) distinguish the physical behavior at the wall from that in the ambient fluid. These prerequisites guarantee that the temperature and velocity profiles match the exponentially stretched sheet's behavior. At the surface, the temperature is set, and the velocity corresponds to the velocity of stretching sheet. The liquid is quiescent far from the sheet, and the heat is becoming close to room temperature. By altering the thermal field close to the surface, source of heat can further affect the temperature distribution of the boundary layer.

3. Dimensional Equations

$$\eta = ye^{\frac{x}{2L}}\sqrt{\frac{u_0}{2\nu L}},\ B = B_0 e^{\frac{x}{2L}},\ u = u_0 e^{\frac{x}{2L}} f'(\eta),$$

$$v = -e^{\frac{x}{2L}}\sqrt{\frac{u_0}{2\nu L}}(f(\eta) + \eta f'(\eta)),\ T = T_\infty + T_0 e^{\frac{x}{2L}}\theta(\eta),$$

$$Q = Q_0 e^{\frac{x}{2L}},\ \theta(\eta) = \frac{T - T_\infty}{T_w - T_\infty},\ M = \frac{\sigma B_0^2}{\rho U_0}\sqrt{\frac{\nu}{U_0 x}},$$

$$K^* = \frac{KU_0}{\nu x},\ \Pr = \frac{\nu}{\alpha} = \frac{\mu c_p}{k},\ Ec = \frac{U_0^2}{c_p(T_w - T_\infty)},\ \beta > 0. \tag{5}$$

Using the above dimensionless scheme (2), (3) and (4) can be reduced in non-dimensional form as follows:

$$\left(1 + \frac{1}{\beta}\right) f''' + ff'' - f'^2 - Mf' - \frac{1}{K'} f' = 0, \tag{6}$$

$$\theta'' + \Pr(f\theta' - f'\theta) + \Pr \cdot Ec \cdot f''^2$$

$$+ \Pr \cdot M \cdot f'^2 + \Pr \cdot Q^*\theta - \frac{Rd}{1 + Rd} \cdot \theta'' = 0. \tag{7}$$

Boundary conditions

$$f(0) = 5,\ \ f'(0) = 1,\ \ \theta(0) = 1,\ \ f'(\infty) \to 0,\ \ \theta(\infty) \to 0. \tag{8}$$

4. Numerical Approach using HAM

We consider the nonlinear ODEs governing the flow and temperature distribution:

$$\left(1 + \frac{1}{\beta}\right) f''' + ff'' - (f')^2 - Mf' - \frac{1}{K'} f' = 0,$$

$$\theta'' + \Pr(f\theta' - f'\theta) + \Pr \cdot Ec \cdot (f'')^2$$

$$+ \Pr \cdot M \cdot (f')^2 + \Pr \cdot Q^*\theta - \frac{Rd}{1 + Rd} \cdot \theta''' = 0.$$

Subject to

$$f(0) = 5, \quad f'(0) = 1, \quad \theta(0) = 1, \quad f'(\infty) \to 0, \quad \theta(\infty) \to 0.$$

Step 1. Parameter initialization

$$\beta = 0.6, \quad M = 0.2, \quad K^* = 0.7, \quad \Pr = 2.5,$$

$$Ec = 0.5, \quad Q^* = 0.9, \quad Rd = 1, \quad S = 0,$$

$$A = 1 + \frac{1}{\beta}, \quad \lambda = \frac{1}{1 + Rd}.$$

Step 2. Initial guesses

$$f_0(\eta) = S + (1 - S)(1 - e^{-\eta}),$$

$$\theta_0(\eta) = e^{-\eta}.$$

Step 3. Construction of nonlinear operators

$$\mathcal{N}_f(f_0) = Af_{0'''} + f_0 f_{0''} - (f_{0'})^2 - Mf_{0'} - \frac{1}{K^*} f_{0'},$$

$$\mathcal{N}_\theta(f_0, \theta_0) = \Pr(f_0\theta_{0'} - f_{0'}\theta_0) + \Pr \cdot Ec \cdot (f_{0''})^2$$

$$+ \Pr \cdot M \cdot (f_{0'})^2 + \Pr \cdot Q^*\theta_0.$$

Step 4. Deformation equations

$$f_{1'''} = -\mathcal{N}_f, \text{ with } f_1(0) = 0, \quad f_{1'}(0) = 0, \quad f_{1'}(\infty) \to 0,$$

$$\theta_{1''} = -\frac{\mathcal{N}_\theta}{\lambda}, \text{ with } \theta_1(0) = 0, \quad \theta_1(\infty) \to 0.$$

Step 5. First-order approximations

$$f(\eta) \approx f_0(\eta) + f_1(\eta),$$

$$\theta(\eta) \approx \theta_0(\eta) + \theta_1(\eta).$$

5. Shear Stress and Rate of Heat Transfer

The rate of heat transfer and wall skin friction play a key role in evaluating drag forces in systems such as pipelines, marine vessels, and aircraft where minimizing friction enhances energy efficiency and operational performance. Conversely, it quantifies the relative effectiveness of convective heat transfer compared to conduction and serves as an essential parameter in managing heat in systems such as heat exchangers, electronic cooling devices, and solar collectors. These parameters are particularly valuable in applications involving polymer extrusion, biomedical flows, and fluid transport through porous media, as they reveal how surface interactions, fluid characteristics, and external influences—such as magnetic fields or porous resistance—affect flow dynamics and thermal transport. Thus, a thorough understanding and accurate regulation of both parameters are crucial for enhancing efficiency, reliability, and energy utilization across diverse engineering and scientific applications.

Shear stress (C_f) and Nusselt number (Nu_θ) equations are as follows:

$$C_f = -\left(1+\frac{1}{\beta}\right) f''(0), \quad Nu_\theta = -\left(1+\frac{4R}{3}\right)\theta'(0). \tag{9}$$

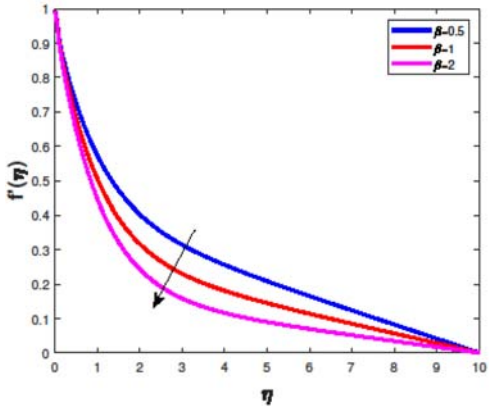

Figure 2. Velocity profile of Casson fluid.

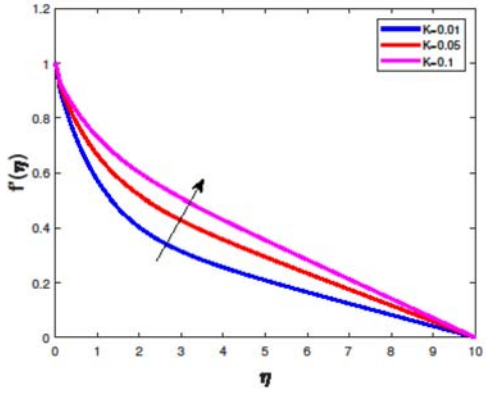

Figure 3. Velocity profile of porous media.

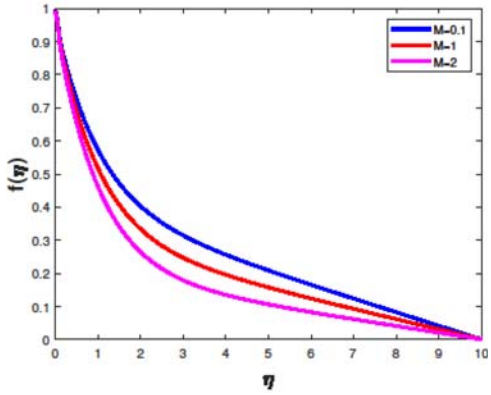

Figure 4. Velocity profile of magnetic field.

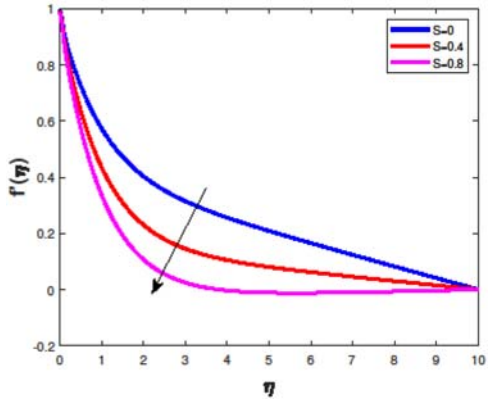

Figure 5. Velocity profile of suction parameter.

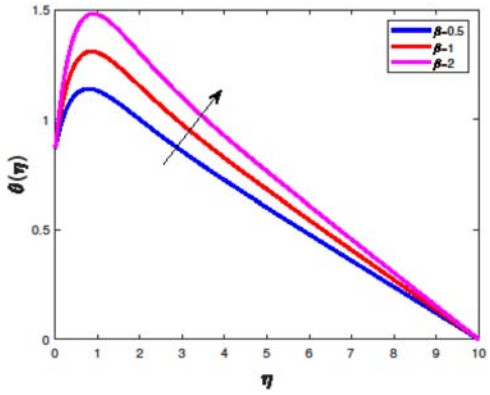

Figure 6. Temperature profile of Casson fluid.

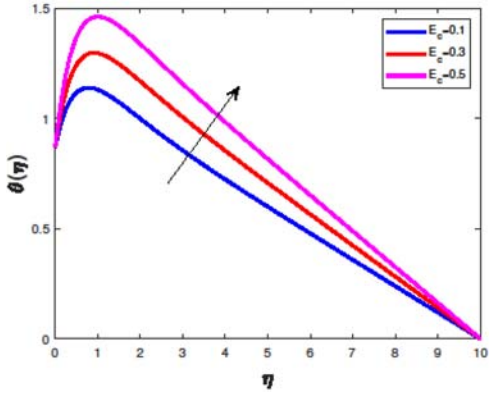

Figure 7. Temperature profile of Eckert number.

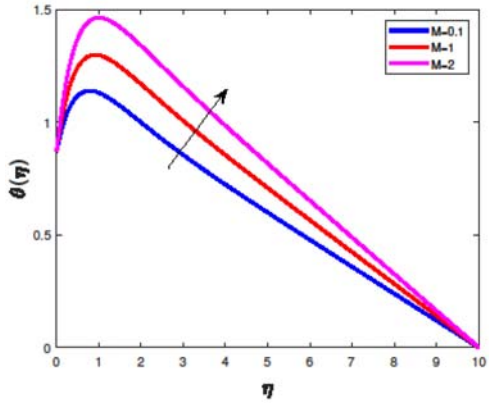

Figure 8. Temperature profile of magnetic field.

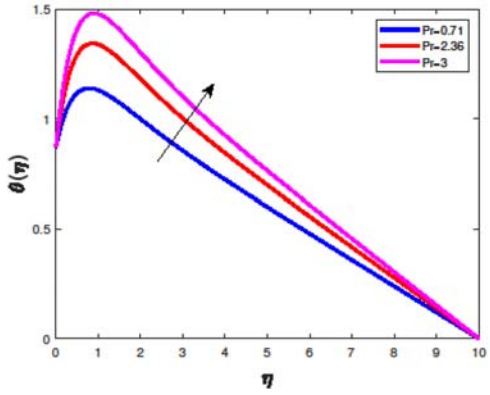

Figure 9. Temperature profile of Prandtl number.

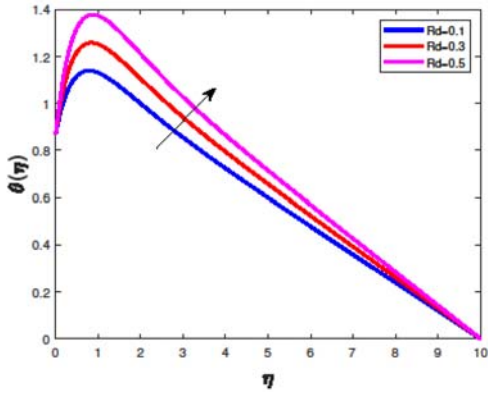

Figure 10. Temperature profile of radiation parameter.

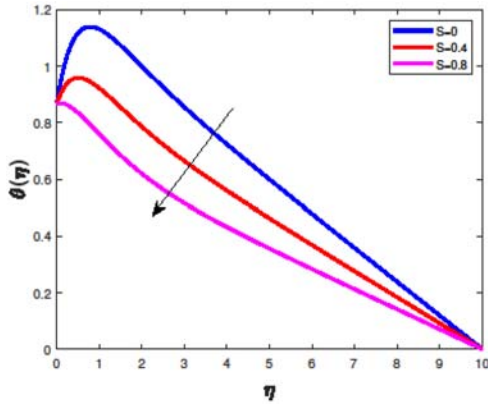

Figure 11. Temperature profile of suction parameter.

Table 1. Variation of skin friction coefficient

M	K	β	$f''(0)$	$Cf\sqrt{\mathrm{Re}_x}$
0.0	0.01	0.5	2.492	-7.476
0.0	0.01	1.0	2.492	-4.984
0.0	0.01	2.0	2.492	-3.738
0.0	0.05	0.5	2.46	-7.38
0.5	0.01	0.5	2.192	-6.576
0.5	0.01	1.0	2.192	-4.384
0.5	0.01	2.0	2.192	-3.288
0.5	0.05	0.5	2.16	-6.48
0.8	0.01	0.5	2.012	-6.036
0.8	0.01	1.0	2.012	-4.024
0.8	0.01	2.0	2.012	-3.018
0.8	0.05	0.5	1.98	-5.94

Table 2. Variation of Nusselt number

Pr	Ec	β	Rd	$\theta'(0)$	Nu_θ
0.71	0.1	0.5	0.1	0.8796	-0.9969
0.71	0.1	0.5	0.3	0.8496	-1.1894
0.71	0.1	0.5	0.5	0.8196	-1.366
0.71	0.1	1.0	0.1	0.9296	-1.0535
2.36	0.3	0.5	0.1	1.0719	-1.2151
2.36	0.3	0.5	0.3	1.0419	-1.4578
2.36	0.3	0.5	0.5	1.0119	-1.6865
2.36	0.3	1.0	0.1	1.1219	-1.2725
3.0	0.5	1.0	0.5	1.0894	-1.7947
3.0	0.5	2.0	0.1	1.1744	-1.3317
3.0	0.5	2.0	0.3	1.1444	-1.591
3.0	0.5	2.0	0.5	1.1144	-1.8318

Table 3. Comparison between the existing model and the proposed model when radiation (RD), viscous dissipation (EC), and magnetic field (M) are neglected

Pr	Existing model, i.e., Vinod et al. [7]	Proposed model
0.71	0.8231	0.8145
1.00	0.9425	0.9425
2.00	1.1768	1.1746
3.00	1.3104	1.3104
5.00	1.5049	1.5049
7.00	1.6123	1.61230

6. Results and Discussion

This section presents the analytical results for the magnetohydrodynamic (MHD) boundary layer flow and heat transfer behavior of a Casson fluid over an exponentially stretching surface. The homotopy analysis method (HAM) is employed to solve the nonlinear ordinary differential equations derived from the governing equations through similarity transformations. The effects of key physical parameters—such as the Hartmann number, Casson fluid parameter, thermal radiation, magnetic dissipation, viscous dissipation, and heat source/sink on the velocity and temperature profiles are thoroughly investigated. The influence of these parameters is illustrated graphically in Figures 2-11, highlighting their roles in modulating flow characteristics and thermal performance.

Figure 2 illustrates the influence of the Casson fluid parameter on velocity variations within the flow, as represented by the velocity profile $f'(\eta)$. As (β) raises, the velocity profile decreases, indicating a reduction in fluid motion. A smaller (β) corresponds to stronger non-Newtonian (shear-thinning) behavior, which increases resistance to flow near the wall.

Figure 3 illustrates that the permeability of the porous media resistance (K) increases with velocity distribution. Figure 4 depicts how the magnetic field affects the velocity distribution. Enhancing (M) falls the speed throughout the layer of the boundary due to the force of the Lorentz. This

resistive electromagnetic force opposes the fluid motion, resulting in a retardation effect that leads to boundary layer thickening. This phenomenon is characteristic of MHD flows and has implications for controlling fluid flow in electrically conducting fluids. Figure 5 shows the impact of (S) on velocity. As *S* increases, the velocity decays more rapidly with (η), leading to a thinner boundary layer. Suction removes fluid from the boundary layer, stabilizing it and enhancing shear near the surface. This effect is often utilized in boundary layer control and thermal regulation. Figure 6 illustrates the effect of the Casson parameter β on the temperature distribution $\theta(\eta)$. As the (β) increases, the temperature profile also rises. The fluid behaves less resistive to deformation and the momentum transfer improves, reducing internal resistance. As a result, thermal diffusion becomes more pronounced, producing a higher temperature distribution throughout the boundary layer.

Figure 7 reveals that the Eckert number (Ec), which measures viscous dissipation. An increase in (Ec) results in higher liquid temperature, as more mechanical energy is converted into thermal energy. This leads to an increase in the thickness of the thermal boundary layer and lower temperature gradients at the surface, indicating a slower heat transfer rate.

Figure 8 examines the effect of magnetic parameter *M* on temperature. Increasing *M* boosts the fluid temperature through resistive (Joule) heating generated by the Lorentz force. This effect thickens the thermal boundary layer and minimizes the surface temperature differential, which might be useful in thermal management of MHD flows. Figure 9 demonstrates the influence of the Prandtl number (Pr) on the thermal profile. As Pr increases, the temperature profile steepens, indicating a thinner thermal boundary layer. Since higher (Pr) values represent fluids with lower thermal diffusivity, heat diffuses more slowly, enhancing the wall rate of heat transfer and enhancing the Nusselt number. Figure 10 elucidates the impact of the thermal radiation Rd. An increase in Rd leads to higher fluid temperatures and a thicker thermal boundary layer. Radiation acts as a heat sink, reducing the gradient of temperature at the wall. This results in a lower Nusselt number, indicating a decrease in surface heat transfer. Figure 11 depicts the temperature

variation with respect to the suction parameter *S*. As suction increases, the temperature profile decreases faster, indicating a narrowing of the heat boundary layer. Suction improves thermal removal from the surface by increasing the wall temperature gradient and thermal performance.

Table 1 presents the variation of the $(Cf\sqrt{\mathrm{Re}_x})$ and the dimensionless gradient of velocity at the wall $f''(0)$ for different values of the *M*, *K* and (β). From the above table, it is observed that the shear stress coefficient $(Cf\sqrt{\mathrm{Re}_x})$ falls in magnitude with enhancing values of (M), (K) and (β). Specifically, as the magnetic parameter (M) increases from 0.0 to 0.8, both $f''(0)$ and $(Cf\sqrt{\mathrm{Re}_x})$ decrease significantly. This pattern suggests that a greater magnetic field restricts fluid motion near the wall because of the Lorentz effect, which serves as a force of resistive against the flow and so reduces shear stress at the boundary. Similarly, an increase in the porosity parameter *K* from 0.01 to 0.05 causes a slightly-reduces in the Shear stress coefficient. This is attributed to the fact that a more porous space offers less resistance to the fluid flow, allowing it to penetrate through the medium more easily, which reduces the gradient of velocity and consequently the wall shear stress. The slip parameter also influences the skin friction significantly. As (β) increases from 0.5 to 2.0, the magnitude of $(Cf\sqrt{\mathrm{Re}_x})$ decreases. This behavior is expected since a higher slip parameter corresponds to a greater velocity slip at the boundary, reducing the velocity gradient $f''(0)$ and thus lowering the shear stress. Notably, the values of $f''(0)$ remain constant for different β values at fixed *M* and *K*, suggesting that in this particular model or numerical solution, $f''(0)$ is not sensitive to changes in slip parameter or is considered at a fixed reference condition. Finally, the results demonstrate that increasing magnetic field strength, permeability, and wall slip act to decrease the skin friction coefficient, which could be advantageous in applications where minimizing drag or wall shear stress is desired.

From Table 2, it is observed that the modifications of the Nu_θ for various values of Pr, Ec, Casson liquid, and Rd. The Nusselt number is a dimensionless measure of convective heat transfer from the surface, and it is defined here as $Nu_\theta = -\left(1 + \frac{4}{3}Rd\right)\theta'(0)$. It is noticed that as the thermal radiation Rd enhances, the heat transfer rate reduces for fixed Pr, Ec and β. This is due to the increased radiative heat flux, which enhances the thermal layer of boundary thickness and falls the walls of gradient of heat. The impact of Ec, which accounts for viscous dissipation, is also significant. An increase in Ec leads to a lessen in $\theta'(0)$ and hence a reduction in Nu_θ. This is because viscous heating increases the fluid temperature near the wall, reducing the effective thermal gradient. Regarding the Casson parameter, it is observed that increasing β leads to an increase in $\theta'(\eta)$, which corresponds to a slightly higher Nu_θ. Physically, higher β values reduce the non-Newtonian effects, allowing for greater thermal diffusion. Finally, increasing Pr that enhances the heat transfer rate. Here is a refined version of your sentence: A high Pr signifies low thermal diffusivity, leading to a thinner thermal layer boundary and a steeper thermal gradient at the wall. This is evident when comparing values such as $Nu_\theta = -1.0535$ at $\Pr = 0.71$, versus $Nu_\theta = -1.7947$ at $\Pr = 3.0$ for similar other conditions. Therefore, thermal radiation and viscous dissipation reduce the heat transfer rate, while higher Prandtl number and weaker non-Newtonian behavior (larger β) enhance surface heat transfer. These trends are consistent with classical boundary layer transfer of heat theory.

Table 3 provides a comparative analysis of the temperature gradient at the wall, represented by $\theta'(0)$, for various values of (Pr), between the base model presented by Vinod et al. [7] and the present extended model. In both cases, the thermal radiation (Rd), viscous dissipation (Ec), and magnetic effects (M) are neglected to isolate the influence of Pr. It is evident that the values of $\theta'(0)$ in the present study closely match those in the base model across all Pr values, validating the accuracy of the extended formulation

under simplified thermal conditions. The minimal differences observed for lower Prandtl numbers (e.g., $\mathrm{Pr} = 0.71$) may be attributed to additional resistance due to porous medium effects introduced in the present model, which slightly thicken the heat boundary layer and reduce the gradient of temperature. As Pr increases, both models show a consistent rise in $-\theta'(0)$ values. This behavior is physically predictable, as increases in Pr values suggest a fall in diffusivity of heat, which leads to a thinner thermal boundary layer and a steeper gradient of temperature at the wall, thereby facilitating transfer of heat.

7. Conclusion

The coupled nonlinear ordinary differential equations, obtained from the unsteady boundary layer formulation of Casson fluid flow incorporating magnetic and porous medium effects, are analytically solved using the homotopy analysis method (HAM). This semi-analytical technique offers a powerful framework for solving strongly nonlinear problems by constructing a convergent series solution. The boundary conditions are applied to the similarity-transformed equations, and convergence control parameters are carefully selected to ensure accurate and stable solutions. A comprehensive parametric analysis is carried out to investigate the effects of key physical parameters such as the Casson fluid parameter (β), magnetic parameter (M), porous medium permeability (K), Prandtl number (Pr), Eckert number (Ec), and the unsteadiness parameter (A) on the dimensionless velocity and temperature distributions. The following are the major conclusions derived from the analysis:

• The magnetic field (M) suppresses fluid velocity but enhances temperature through Joule heating.

• Porous medium resistance (K) reduces flow velocity and modifies thermal gradients.

• Thermal slip (γ) decreases the surface heat transfer rate.

• Higher Prandtl number (Pr) leads to reduced thermal diffusivity and thinner thermal boundary layers.

• Radiation parameter (Rd) and heat generation enhance the fluid temperature near the wall.

• Shear stress and rate of heat transfer are highly sensitive to Casson parameter and thermal-magnetic interactions.

• The extended model shows improved accuracy and physical realism over the base model.

• The comparison shows excellent agreement between the present extended model and the base model by Vinod et al. [7] when radiation (Rd), viscous dissipation (Ec), and magnetic field (M) are neglected.

Acknowledgment

The authors would like to express sincere gratitude to their respective institutions for providing necessary facilities and support throughout this research work.

References

[1] I. L. Animasaun, E. A. Adebile and A. I. Fagbade, Casson fluid flow with variable thermo-physical property along exponentially stretching sheet with suction and exponentially decaying internal heat generation using the homotopy analysis method, J. Niger. Math. Soc. 35(1) (2016), 1-17.

[2] B. C. Sakiadis, Boundary-layer behaviour on continuous solid surfaces: I. Boundary-layer equations for two-dimensional and axisymmetric flow, AIChE J. 7(1) (1961), 26-28.

[3] P. S. Gupta and A. S. Gupta, Heat and mass transfer on a stretching sheet with suction or blowing, Can. J. Chem. Eng. 55(6) (1977), 744-746.

[4] S. Mukhopadhyay and R. S. R. Gorla, Effects of partial slip on boundary layer flow past a permeable exponential stretching sheet in presence of thermal radiation, Heat Mass Transf. 48(10) (2012), 1773-1781.

[5] B. Tashtoush and M. Al-Odat, Magnetic field effect on heat and fluid flow over a wavy surface with a variable heat flux, J. Magn. Magn. Mater. 268(3) (2004), 357-363.

[6] M. Sajid and T. Hayat, Influence of thermal radiation on the boundary layer flow due to an exponentially stretching sheet, Int. Commun. Heat Mass Transf. 35(3) (2008), 347-356.

[7] Y. Vinod, K. R. Raghunatha, S. N. Nagappanavar, N. Nazarova and M. Gupta, Boundary layer flow of a non-Newtonian fluid over an exponentially stretching sheet with the presence of a heat source/sink, J. Partial Differ. Equ. Appl. Math. 2025, Article ID 101111.

[8] S. Mukhopadhyay, P. R. De, K. Bhattacharyya and G. C. Layek, Casson fluid flow over an unsteady stretching surface, Ain Shams Eng. J. 4(4) (2013), 933-938.

[9] A. Ishak, MHD boundary layer flow due to an exponentially stretching sheet with radiation effect, Sains Malays. 40(4) (2011), 391-395.

[10] K. Bhattacharyya, Steady boundary layer flow and reactive mass transfer past an exponentially stretching surface in an exponentially moving free stream, J. Egypt. Math. Soc. 20(3) (2012), 223-228.

[11] T. Hayat, M. Imtiaz, A. Alsaedi and R. Mansoor, MHD flow of nanofluids over an exponentially stretching sheet in a porous medium with convective boundary conditions, Chin. Phys. B 23(5) (2014), 054701.

[12] K. Vajravelu, Flow and heat transfer in a saturated porous medium over a stretching surface, ZAMM – J. Appl. Math. Mech. 74(12) (1994), 605-614.

[13] Z. Abbas, M. Sajid and T. Hayat, MHD boundary-layer flow of an upper-convected Maxwell fluid in a porous channel, Theo. Comput. Fluid Dyn. 20(4) (2006), 229-238.

[14] I. Ahmad, M. Sajid, W. Awan, M. Rafique, W. Aziz, M. Ahmed, A. Abbasi and M. Taj, MHD flow of a viscous fluid over an exponentially stretching sheet in a porous medium, J. Appl. Math. 2014, Article ID 256761.

[15] D. Srinivasacharya and P. Jagadeeshwar, Effect of Joule heating on the flow over an exponentially stretching sheet with convective thermal condition, Math. Sci. 13 (2019), 201-211.

[16] S. Mukhopadhyay, K. Bhattacharyya and G. C. Layek, Steady boundary layer flow and heat transfer over a porous stretching sheet in presence of thermal radiation, Int. J. Heat Mass Transf. 54(13-14) (2011), 2751-2757.

[17] I. Ullah, S. Shafie, I. Khan and K. L. Hsiao, Brownian diffusion and thermophoresis mechanisms in Casson fluid over a moving wedge, Results Phys. 9 (2018), 183-194.

[18] E. Elbashbeshy, T. G. Emam and K. M. Abdelgaber, Effects of thermal radiation and magnetic field on unsteady mixed convection flow and heat transfer over an exponentially stretching surface with suction in the presence of internal heat generation/absorption, J. Egypt. Math. Soc. 20(3) (2012), 215-222.

[19] T. Hayat, A. Shafiq, A. Alsaedi and S. A. Shahzad, Unsteady MHD flow over exponentially stretching sheet with slip conditions, Appl. Math. Mech. 37(2) (2016), 193-208.

[20] A. Hussain, M. Y. Malik, T. Salahuddin, S. Bilal and M. Awais, Combined effects of viscous dissipation and Joule heating on MHD Sisko nanofluid over a stretching cylinder, J. Mol. Liq. 231 (2017), 341-352.